Bull. Mater. Sci., Vol. 36, No. 1, February 2013, pp. 121–128. © Indian Academy of Sciences.

In situ ring-opening polymerization of hydroxyapatite/poly(ethylene adipate)-*co*-(ethylene terephthalate) biomimetic composites

PUNNAMA SIRIPHANNON* **and PATHAVUTH MONVISADE**

Department of Chemistry, Faculty of Science, King Mongkut's Institute of Technology Ladkrabang, Chalongkrung Road, Ladkrabang, Bangkok 10520, Thailand

MS received 10 July 2011; revised 29 August 2011

Abstract. Hydroxyapatite/poly(ethylene adipate)-*co*-poly(ethylene terephthalate) biomaterials (HAp/PEA-*co*-PET) have been prepared by ring opening polymerization (ROP) of cyclic oligo(ethylene adipate)-*co*-oligo(ethylene terephthalate) (C-OEA-*co*-C-OET) in the porous hydroxyapatite (HAp) scaffolds at 250 °C for 24 h under vacuum. The content of ROP-PEA-*co*-PET in the HAp/PEA-*co*-PET composite was about 20 wt% with the values of number average molecular weight ($\overline{M}_n$) and weight average molecular weight ($\overline{M}_W$) of 3380 and 7160 g/mol, respectively. Compressive strength and modulus of the HAp/PEA-*co*-PET composites were about 29 and 246 MPa, respectively. These mechanical properties were higher than those of the porous HAp templates and natural cancellous bone. *In vitro* bioactivity of the HAp/PEA-*co*-PET composites was studied by soaking in simulated body fluid (SBF) under the flowing system at the rate of 130 mL/day for 7, 14, 21 and 28 days. The formation of hydroxyapatite nanocrystals was observed on the composite surfaces through the consumption of calcium and phosphorus from the SBF solution, indicating the bioactivity of these HAp/PEA-*co*-PET composites. These results indicated the competency of HAp/PEA-*co*-PET composites for biomedical applications.

Keywords. Hydroxyapatite; ring-opening polymerization; copolyester; biomaterials; nanocrystal.

1. Introduction

Bones serve various functions in human body, such as the body's supporting framework, providing muscle-attachment points for movement, protecting the internal organs, etc. The bones are mainly composed of highly interconnected hard inorganic minerals of calcium phosphate and soft organic tissues (Park 1979). Many researchers attempted to synthesize and develop various hydroxyapatite (HAp)–polymer composites which mimic the natural bone system, e.g. HAp-collagen (Wahl *et al* 2007; Song *et al* 2008; Touny *et al* 2010), -chitosan (Ge *et al* 2010; Ezhova *et al* 2011), -poly(methyl methacrylate) (Monvisade *et al* 2007; Tham *et al* 2010). These composites combine the advantages of ceramics and polymers, resulting in the biocompatible materials with better structural integrity and flexibility than the pure HAp.

Among various kinds of polymers, polyesters are one of the most attractive polymers used in biomedical applications because they possess a very wide range of mechanical properties and bioactivity, depending on their structures and functional groups. Various aliphatic polyesters like polyglycolic acid (PGL) (Vainionpää 1985; Antikainen *et al* 1992; Chen *et al* 2007), polylactic acid (PLA) (Antikainen *et al* 1992; Chen *et al* 2007; Kitajima *et al* 2010) and their copolyesters (PLGA) (Kim *et al* 2006; Chung *et al* 2006; Hayakawa *et al* 2009) are widely used for a number of different medical applications due to their biodegradability. These biodegradable polyesters serve a temporary mechanical or therapeutic function, in which they will gradually degrade and be replaced by the surrounding tissues after prolonged implantation. On the other hand, the aromatic polyesters, e.g. polybutylene terephthalate (PBT) (Joe and Kim 1990; Risbud *et al* 2001), possess high mechanical properties and biocompatibility, however, they are bioinert in physiological environments. From this point of view, various tailor-made composites with different properties for different medical applications can be designed from different polyesters.

In this study, we developed a new composite between HAp and aliphatic-aromatic copolyester, i.e. poly(ethylene adipate)-*co*-poly(ethylene terephthalate) copolyesters (PEA-*co*-PET). This copolyester was selected because it contained an aromatic ester unit of PET and aliphatic ester unit of PEA, which could behave as a thermoplastic elastomer, imparting high flexibility and strength of the composites. The composites were prepared by ring opening polymerization (ROP) of cyclic oligo(ethylene adipate)-*co*-oligo(ethylene terephthalate) (C-OEA-*co*-C-OET) in the porous HAp templates. The HAp/PEA-*co*-PET composites and the ring-opening polymerized products were characterized by various techniques.

2. Experimental

2.1 *Preparation of porous hydroxyapatite (HAp) scaffolds*

HAp was prepared by co-precipitation of calcium hydroxide ($Ca(OH)_2$) and phosphoric acid (H_3PO_4) as reported

*Author for correspondence (kspunnam@kmitl.ac.th)

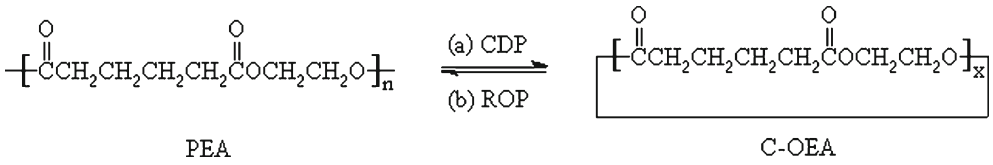

Scheme 1. Cyclo-depolymerization (CDP) of PEA and ring-opening polymerization (ROP) of C-OEA.

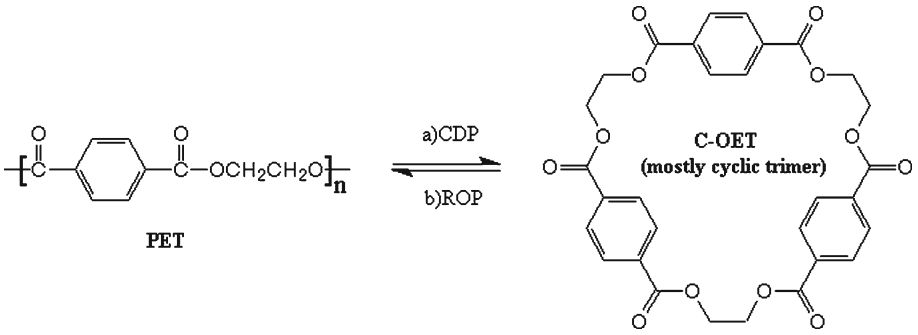

Scheme 2. Cyclo-depolymerization (CDP) of PET and ring-opening polymerization (ROP) of C-OET.

previously (Monvisade *et al* 2007). The co-precipitated powder was calcined at 500 °C for 2 h. An aqueous solution of poly(vinyl alcohol) (PVA) binder was prepared with a concentration of 100 g/L. The calcined HAp powder was dispersed in the PVA solution and then left to set a cake. The cake was then cut into rectangular shape with a dimension of $1 \times 1 \times 1$ cm^3. The HAp cubes were fired at 1100 °C for 5 h in order to eliminate the PVA, creating the porous HAp templates. Crystalline structure and morphology of the HAp templates were analysed by X-ray diffractometer (XRD; Bruker AG, D8 Advance) and scanning electron microscope (SEM; LEO, LEO1455VP), respectively.

2.2 *Preparation of cyclic oligomers*

2.2a *Cyclic oligo(ethylene adipate) (C-OEA)*: The poly(ethylene adipate) (PEA) precursor was prepared by condensation polymerization of dimethyl adipate (DMA) and ethylene glycol (EG) using tetraisopropyl orthotitanate catalyst (0·5 wt% of DMA) at 170 °C under nitrogen atmosphere for 24 h. PEA precursor (5 g) and tetraisopropyl orthotitanate catalyst (3 mol% of PEA) were dissolved in chlorobenzene under high dilution condition and then cyclo-depolymerized (CDP) by heating under reflux temperature for 7 days. The CDP reaction of PEA is shown in scheme 1. This mixture was rotary evaporated and then dried in an oven at 60 °C for 24 h to obtain the C-OEA cyclic product.

2.2b *Cyclic oligo(ethylene terephthalate) (C-OET)*: The commercially available PET (5 g) and tetraisopropyl orthotitanate catalyst (3 mol% of PET) was dissolved in ortho-dichlorobenzene under high dilution condition. The mixture was refluxed for 4 days in order to get cyclo-depolymerized PET as shown in scheme 2, resulting in the C-OET cyclic oligomer.

2.2c *Cyclic oligo(ethylene adipate)-co-oligo(ethylene terephthalate) (C-OEA-co-C-OET)*: The mixture, having 1:1 molar ratio of C-OEA:C-OET, was dissolved in ortho-dichlorobenzene with dibutyl tinoxide catalyst (3 mol% with respect to cyclics). The mixture was refluxed for 7 days in order to obtain the co-cyclic of C-OEA-*co*-C-OET and then dried in an vacuum oven for 24 h.

2.2d *Characterization of cyclic oligomers*: The C-OEA, C-OET and C-OEA-*co*-C-OET were characterized by ^{1}H-NMR (Bruker AG, NMR 300 ULTRA SHIELD) using tetramethylsilane (TMS) as internal standard. The number of average molecular weight ($\overline{M}_n$), weight average molecular weight ($\overline{M}_W$) and molecular weight distribution (MWD) of C-OEA, C-OET and C-OEA-*co*-C-OET were determined by gel permeation chromatography (GPC; Millipore, WATER 150-cv) using tetrahydrofuran (THF) as the mobile phase at a flow rate of 1 mL/min.

2.3 *Preparation of HAp/PEA-co-PET composites*

The as prepared C-OEA-*co*-C-OET and 3 mol% of dibutyl tinoxide were dissolved in dichloromethane. The porous HAp templates were immersed into the C-OEA-*co*-C-OET solution for 24 h to allow almost co-cyclic molecules penetrating into the porous structure of HAp templates. After removal of the solvent, the HAp/C-OEA-*co*-C-OET pre-composites were *in situ* ring-opening polymerized (ROP) at

Table 1. Ion concentrations of simulated body fluid and human blood plasma (Kokubo and Takadama 2006).

	Ion concentration (mM)						
	Na^+	K^+	Mg^{2+}	Ca^{2+}	Cl^-	HCO_3^-	HPO_4^{2-}
Simulated body fluid	142·0	5·0	1·5	2·5	148·8	4·2	1·0
Human blood plasma	142·0	5·0	1·5	2·5	103·0	27·0	1·0

250 °C for 24 h under vacuum to obtain the HAp/PEA-*co*-PET composites.

The HAp/PEA-*co*-PET composites were characterized in comparison with the porous HAp templates using XRD and SEM. The weight percentage of the ring-opening polymerized PEA-*co*-PET (ROP-PEA-*co*-PET) in the composites was determined by thermogravimetric analysis (TGA; Perkin Elmer, Pyris 1 TGA), in which the inner fractions of composites were heated from 50 to 750 °C at a heating rate of 10 °C/min. The ROP-PEA-*co*-PET was extracted from the composite blocks by immersing in chloroform for 24 h and then characterized by ^{1}H-NMR using TMS as internal standard and Fourier transform infrared spectrometer (FT–IR; Bruker AG, IFS28) using KBr disc. The molecular weights and MWD of the ROP-PEA-*co*-PET were determined by GPC using the same condition as the C-OEA, C-OET and C-OEA-*co*-C-OET precursors. Melting temperature (T_m) and glass transition temperature (T_g) were determined using DSC (Pyris Diamond DSC, Perkin-Elmer).

2.4 *In vitro bioactivity testing*

The surfaces of the HAp/PEA-*co*-PET composites were polished using 4 μm diamond paste before *in vitro* testing. The composites were then soaked in simulated body fluid (SBF), having concentrations of inorganic ions similar to those in human blood plasma as shown in table 1 (Kokubo and Takadama 2006). The starting pH of SBF solution was adjusted to 7·4. Each pellet of HAp/PEA-*co*-PET composite was separately set in a closed plastic vessel. The SBF solution was drawn from a supply tank by peristaltic pump at the rate of about 130 mL/day and then flowed through the HAp/PEA-*co*-PET composite in the closed vessel. The composites were soaked in the flowing systems for 7, 14, 21 and 28 days. After each predetermined soaking time, the soaked HAp/PEA-*co*-PET composite was removed from the soaking system, gently washed with distilled water and dried at room temperature. The surfaces of the soaked HAp/PEG composites were investigated by XRD and SEM. Changes of calcium (Ca), phosphorus (P) and carbon (C) concentrations on the composite surfaces were determined by SEM with associated energy dispersive X-ray spectroscopy (EDX; GENESIS2000, EDAX) for microanalysis.

2.5 *Compressive strength and compressive modulus*

Compressive strength and compressive modulus of the HAp/PEA-*co*-PET composites were measured in comparison with the original porous HAp templates. Five samples with dimensions of $\sim 1 \times 1 \times 1$ cm^3 were loaded with a crosshead speed of 2·5 mm/min by universal testing machine (Lloyd Instrument, LR30K) using 30 kN load cell to obtain the average value of compressive strength and compressive modulus along with its standard deviation.

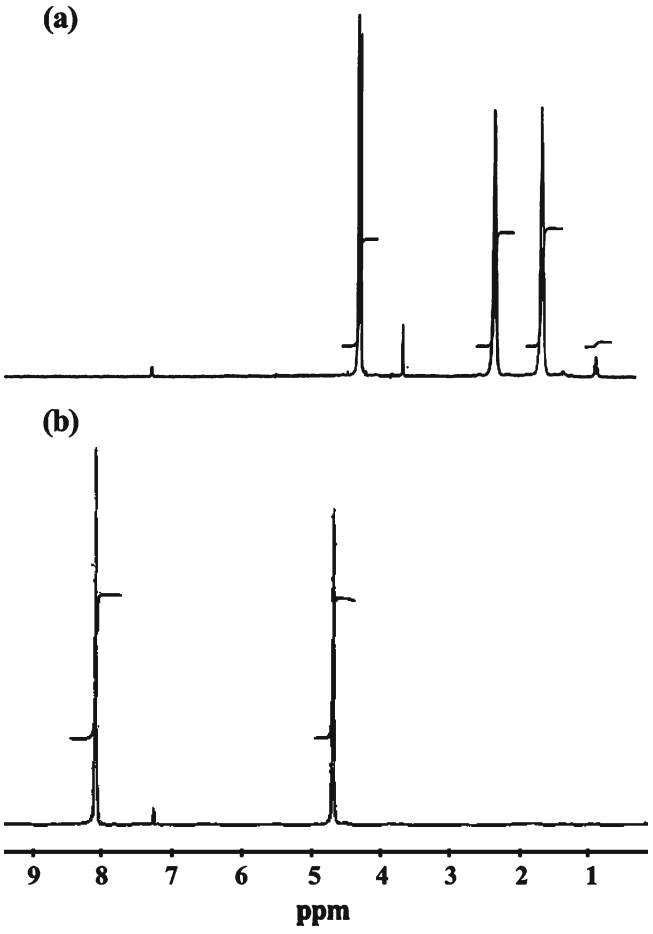

Figure 1. ^{1}H-NMR spectra of (**a**) C-OEA and (**b**) C-OET precursors synthesized *via* cyclodepolymerization reactions.

3. Results and discussion

3.1 *Characterization of starting cyclic oligomers*

Figure 1 shows ^{1}H NMR spectra of C-OEA and C-OET precursors synthesized *via* cyclodepolymerization reactions (schemes 1 and 2). The ^{1}H NMR spectrum of cyclode-

polymerized C-OEA in figure 1(a) showed the signals of methyl groups in the main aliphatic chains at δ 1·7 ppm for $-CH_2\underline{CH_2}\underline{CH_2}CH_2-$, δ 2·4 ppm for $-CO\underline{CH_2}-$ and δ 4·3 ppm for $-O\underline{CH_2}CH_2-$, while, the ^{1}H-NMR spectrum of C-OET in figure 1(b) showed chemical shifts at δ 4·7 ppm for $-O\underline{CH_2}\underline{CH_2}O-$ and δ 8·1 ppm for proton adjacent to aromatic. Both spectra did not show the signal of end groups at δ 4·2 ppm for $-O\underline{CH_2}CH_2OH$ and δ 3·8 ppm for $-OCH_2\underline{CH_2}OH$, indicating the complete cyclodepolymerization of the starting PEA and PET to C-OEA and C-OET cyclics, respectively.

The C-OEA-*co*-C-OET co-cyclic was obtained in 93% yield by refluxing the starting C-OEA and C-OET cyclics in ortho-dichlorobenzene with dibutyl tinoxide catalyst for 7 days. The DSC analyses showed the melting temperature (T_m) of C-OEA-*co*-C-OET to be 179 °C, in which it was different from those of C-OEA ($T_m \sim 20$ °C) and C-OET ($T_m \sim 202$ °C). In addition, the $\overline{M}_W$ and $\overline{M}_n$ of C-OEA-*co*-C-OET co-cyclic were slightly increased from those of the starting cyclics as shown in table 2. These results indicated the formation of a new cyclic having different structure and properties from its starting cyclics.

Figure 2(a) shows ^{1}H NMR spectrum of C-OEA-*co*-C-OET, in which it described the combination of signals corresponding to three different structures as shown in figure 3. The first structure of C-OEA was observed at δ 1·7, 2·4 and 4·3 ppm due to the protons of $-CH_2C\underline{H_2}C\underline{H_2}CH_2-$ (a_1), $-COC\underline{H_2}-$ (a_2) and $-OC\underline{H_2}C\underline{H_2}O-$ (a_3), respectively. The signals at chemical shift δ 4·7 and 8·1 ppm, respectively represented the aromatic protons (b_1) and $-OC\underline{H_2}C\underline{H_2}O-$ (b_2) of C-OET unit. The signals of C-OEA-*co*-C-OET co-cyclic observed at δ 4·4 and 4·5 ppm corresponded to the $-OC\underline{H_2}CH_2O-$ heterolinkage connecting to aliphatic unit (c_1) and $-OCH_2C\underline{H_2}O-$ heterolinkage connecting to aromatic unit (c_2), respectively.

Figure 4(a) shows FT–IR spectrum of C-OEA-*co*-C-OET co-cyclic. The spectrum showed main absorbance peaks at about 2952 cm^{-1} of ν_{C-H}, 1728 cm^{-1} of $\nu_{C=O}$ ester group, 1609 and 1454 cm^{-1} of $\nu_{C=C}$ aromatic group, 1267 and 1101 cm^{-1} of ν_{C-O}, 875 and 730 cm^{-1} of ν_{C-H} aromatic

Table 2. Molecular weights of starting cyclics and ROP-PEA-*co*-PET in HAp/PEA-*co*-PET composites.

Sample	$\overline{M}_W$	$\overline{M}_n$
C-OEA	1270	780
C-OET	760	630
C-OEA-*co*-C-OET	1610	880
HAp/PEA-*co*-PET	7160	3380

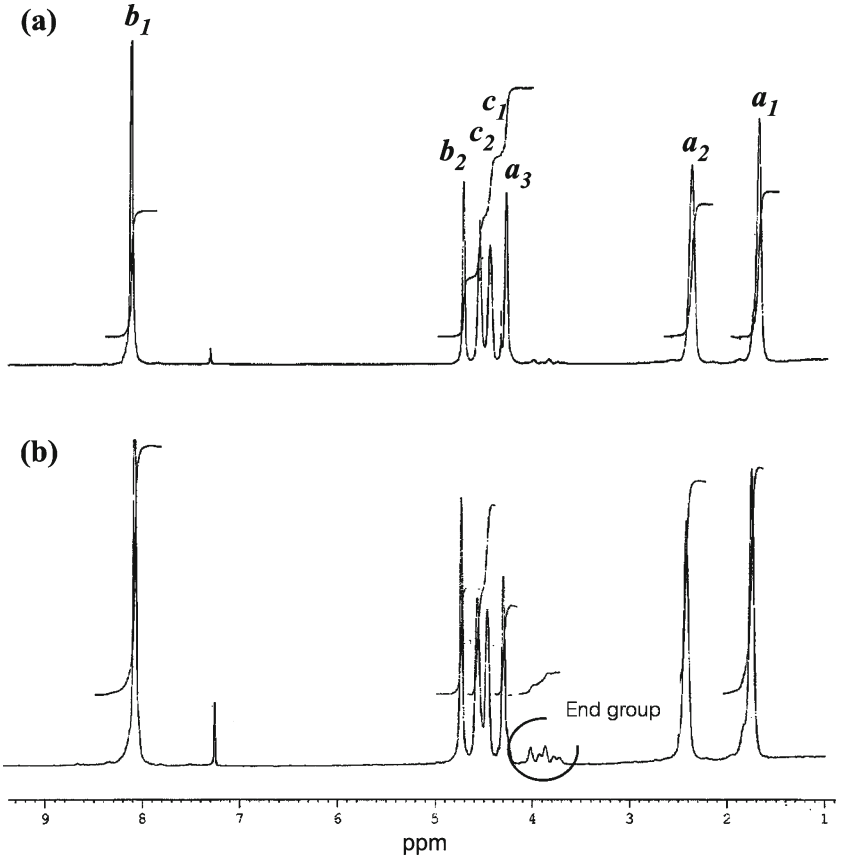

Figure 2. ^{1}H-NMR spectra of (**a**) C-OEA-*co*-C-OET co-cyclic and (**b**) ROP-PEA-co-PET extracted from HAp/PEA-co-PET composites.

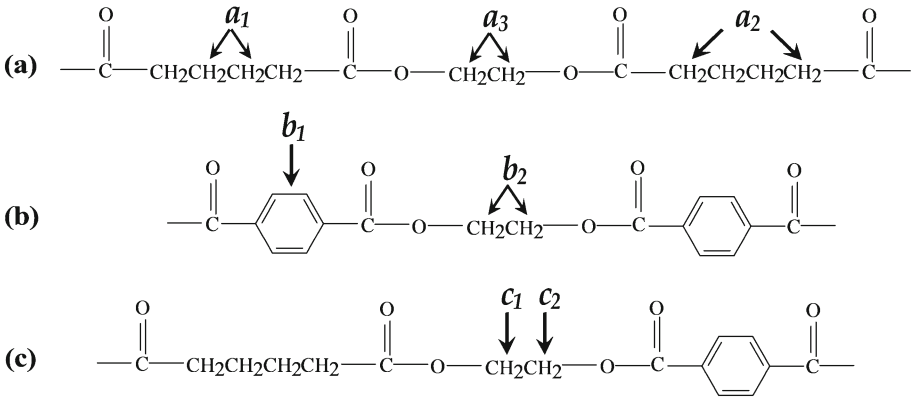

Figure 3. Chemical structures of C-OEA-*co*-C-OET and ROP-PEA-*co*-PET.

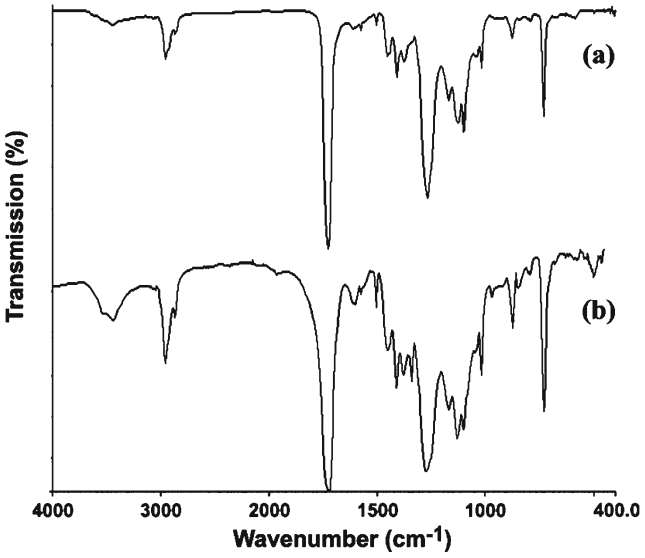

Figure 4. FT–IR spectra of (**a**) C-OEA-*co*-C-OET co-cyclic and (**b**) ROP-PEA-co-PET extracted from HAp/PEA-co-PET composites.

group. All peaks corresponded to three structures proposed in figure 3.

3.2 *HAp/PEA-co-PET hybrid composites*

In the pre-composites, the C-OEA-*co*-C-OET co-cyclic was not only coated on the outer surface but also penetrated into the interior pore of the HAp templates. By heating the pre-composites at 250 °C under vacuum, the co-cyclic was ring-opening polymerized to create the HAp/PEA-*co*-PET composites. The SEM micrographs and EDX data of the HAp templates and HAp/PEA-*co*-PET composites are shown in figures 5(a) and (b), respectively. The HAp templates were observed as the agglomerated grains of HAp with interconnected pores of various sizes generated from the decomposition of PVA. The EDX spectra and elemental mapping of the starting porous HAp template were mainly composed of calcium (Ca) and phosphorus (P). After ROP of the pre-composites, a continuous ROP-PEA-*co*-PET layer was observed to coat on both interior pores and exterior surface of the HAp templates. In addition, the high amount of carbon (C) constituent was detected in the EDX spectra of the HAp/PEA-*co*-PET composites as shown in figure 5(b). The EDX elemental mapping also showed wide area of carbon distribution on the composite surface, insisting the porous HAp was coated with the ROP-PEA-*co*-PET layer. The XRD pattern of the HAp/PEA-*co*-PET composites is shown in figure 6(a). The XRD peaks observed in the HAp/PEA-*co*-PET composites at around $2\theta = 31{\cdot}8°$, $32{\cdot}2°$, $32{\cdot}9°$, $39{\cdot}6°$, $46{\cdot}5°$, $49{\cdot}4°$, $50{\cdot}5°$ and $51{\cdot}2°$ correspond to the crystalline signals of HAp templates. This result was because the signal of thin amorphous ROP-PEA-*co*-PET layer could not obscure the crystalline signal of the HAp templates.

The interior part of the HAp/PEA-co-PET composites was analysed by TGA technique in order to investigate the amount of ROP-PEA-*co*-PET polymerized within the HAp templates from its weight loss percentage. The TGA result corresponded to the ability of C-OEA-*co*-C-OET interpenetrated and ring-opening polymerized in the interior part of the HAp templates. The amount of ROP-product determined by the above mentioned techniques was about 20 wt%.

3.3 *Characterization of ROP-PEA-co-PET*

The ROP-PEA-*co*-PET was extracted from the HAp/PEA-*co*-PET composites by immersing the composites in chloroform for 24 h. The DSC analysis of the extracted ROP-PEA-*co*-PET reveals a single glass transition temperature (T_g) at $-12{\cdot}7$ °C, indicating the ROP-product was random copolymers. In addition, no melting temperature (T_m) was observed in the DSC thermogram of the ROP-product, corroborating the transformation of C-OEA-*co*-C-OET co-cyclic to PEA-*co*-PET by ring-opening polymerization. The GPC data of the extracted ROP-PEA-*co*-PET were shown in table 2 in comparison with those of the starting cyclic oligomers. The $\overline{M}_n$ and $\overline{M}_W$ of the ROP-product were 3380 and 7160 g/mol, respectively in which they were increased from its starting co-cyclic.

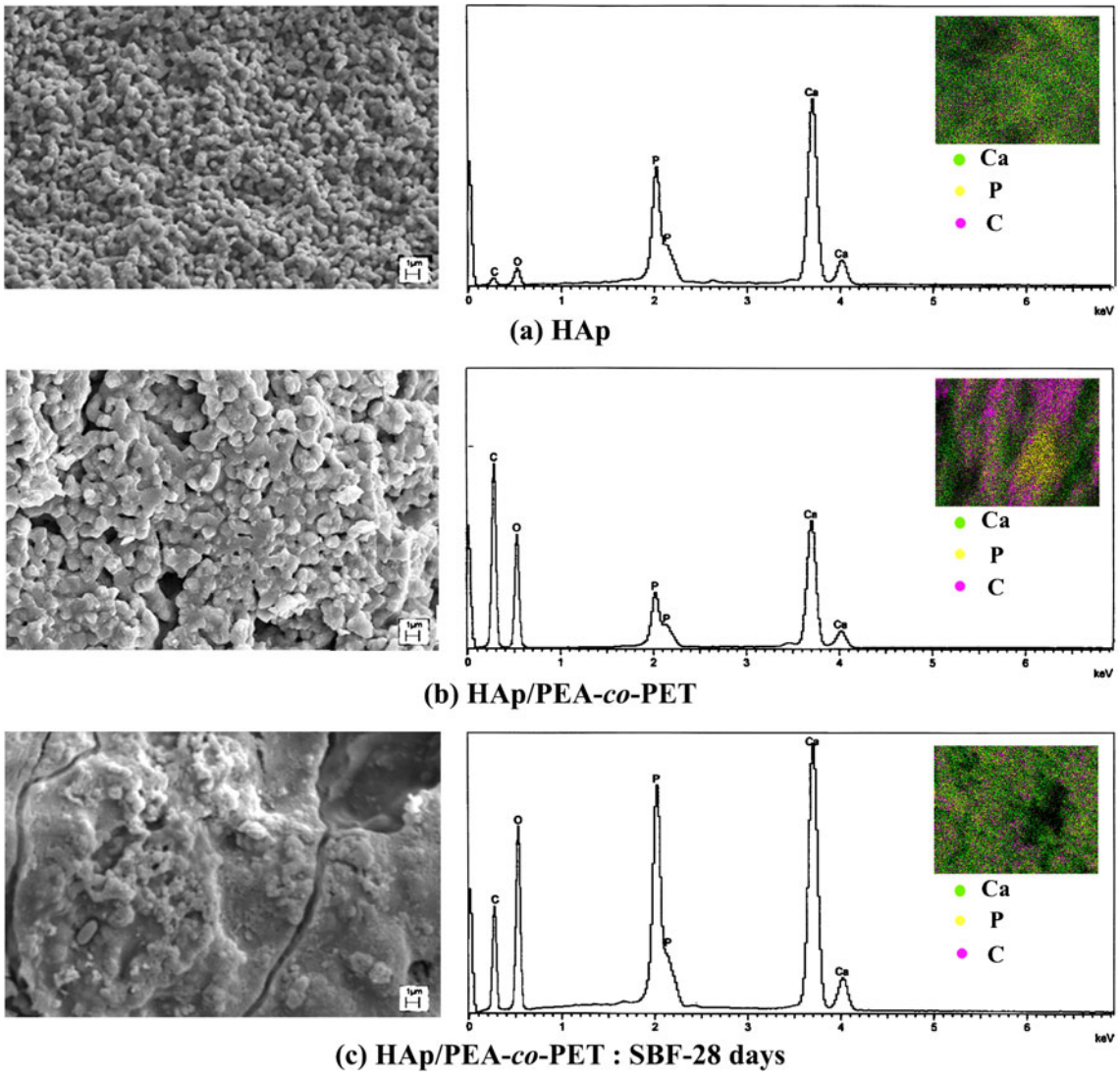

Figure 5. SEM micrographs, EDX spectra and elemental mappings of surfaces of HAp scaffold (**a**), HAp/PEA-*co*-PET composites before soaking in SBF (**b**) and after soaking in SBF for 28 days (**c**).

Figure 2(b) shows ^{1}H-NMR spectra of extracted ROP-PEA-*co*-PET in comparison with the starting co-cyclic. The spectrum mainly consisted of the combination signals of protons from the PEA and PET units, in which the signals of –OC**H**$_2$CH$_2$OH and –OCH$_2$C**H**$_2$OH end groups were clearly observed at δ 4·2 and 3·8 ppm, respectively. These results evidently indicated the successful ring-opening polymerization of C-OEA-*co*-C-OET co-cyclic at 250 °C for 24 h within the porous of HAp templates. In addition, the signals at the chemical shift δ 4·3, 4·4, 4·5 and 4·8 ppm, corresponding to the ethylene units of the copolyesters, were observed in the spectra of ROP-PEA-*co*-PET. These signals indicated that the structure of the ROP-PEA-*co*-PET was random copolyester, in which it consisted of three different kinds of ethylene units in copolyester, including two homolinkages and one heterolinkage similar to its starting co-cyclic as shown in the chemical structures in figure 3. The integration of these chemical shift data indicated the molar ratios of structures (a):(b):(c) to be approximately equal to 5:6:11. The molar ratio of PEA : PET units in ROP-PEA-*co*-PET determined from the ^{1}H-NMR spectrum was equal to 48:52.

Figure 4(b) shows FT–IR spectra of extracted ROP-PEA-*co*-PET. Most of absorbance peaks observed in the extracted ROP-PEA-*co*-PET were similar to its starting co-cyclic. In addition, the broad absorbance peak at ∼3500–3600 cm^{-1} was also observed corresponding to the OH stretching of the ROP-PEA-*co*-PET end group. This observation also insisted the transformation of the starting co-cyclic to the copolyester.

3.4 *In vitro bioactivty of HAp/PEA-co-PET composites*

Figures 6(a)–(e) show XRD patterns of the surfaces of the HAp/PEA-*co*-PET composites before and after soaking in the SBF solution for 7, 14, 21 and 28 days. The main

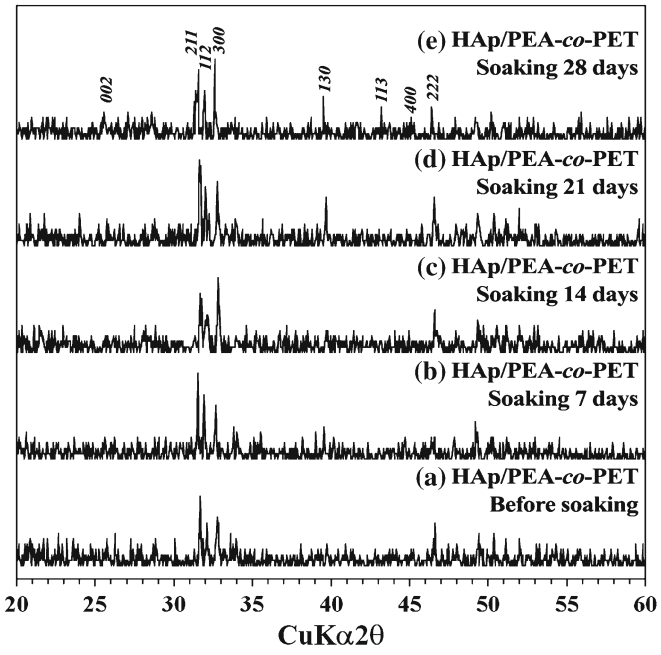

Figure 6. XRD patterns of HAp/PEA-*co*-PET composites before soaking in SBF (**a**) and after soaking in SBF for 7 days (**b**), 14 days (**c**), 21 days (**d**) and 28 days (**e**).

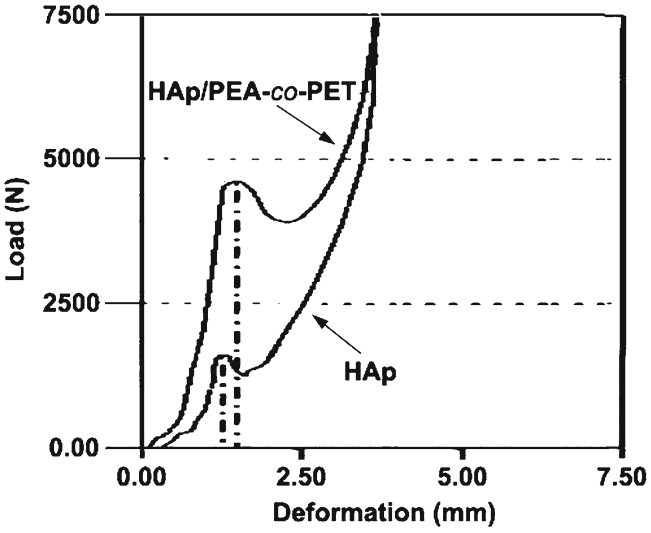

Figure 7. Compressive load-deformation curves of HAp scaffold and HAp/PEA-*co*-PET composite.

crystalline peaks of HAp were observed in all samples at around $2\theta = 31{\cdot}8°$, $32{\cdot}2°$, $32{\cdot}9°$, $39{\cdot}6°$, $46{\cdot}5°$, $49{\cdot}4°$, $50{\cdot}5°$ and $51{\cdot}2°$. After prolonged soaking in the SBF solution, the crystalline peaks in figures 6(b)–(e) were broadened due to the overlapping of the low crystallinity and/or nanocrystallite size of newly formed HAp. The nanocrystallite HAp precipitated on the composite surfaces by consuming the Ca^{2+} and PO_4^{3-} ions from the SBF solution. After prolonged soaking for 14–28 days, the crystalline peaks at $2\theta = 32{\cdot}9°$ corresponded to 3 0 0 plane which was apparently larger, which indicated the preferential crystal plane of the long axis which can be defined as the *a*-plane. The growth of HAp nanocrystals along the *a*-plane was considered to be a result of laminar flow of SBF during *in vitro* bioactivity testing. These results differed from the 0 0 2 preferred orientation of HAp nanocrystal grown in the static SBF solution as previously reported (Siriphannon *et al* 2002).

Change of the surface characteristics of the soaked HAp/PEA-*co*-PET composites observed by SEM with associated EDX is shown in figure 5(c). After prolonged soaking in SBF solution for 28 days, the HAp/PEA-*co*-PET surface was observed to be coated by a newly formed layer of cauliflower-like particles, consisting of the agglomerated nanocrystals. The EDX spectra indicated that the main compositions of cauliflower-like layer were Ca and P with the Ca/P molar ratio of 1·4, while the C content of ROP-PEA-*co*-PET was slightly detected. The EDX result affirmed that the cauliflower-like nanocrystals were the newly precipitated HAp layer. The elemental mapping in figure 5(c) exhibited the distributions of Ca and P throughout the composite surface, indicating the formation of thick regular HAp layer coated on the composite surface. In addition, the cauliflower-like particles formed in the flowing system of SBF solution were smaller than those normally formed in the static system previously reported elsewhere (Siriphannon *et al* 2002). This result was attributed to the effect of the fresh SBF solution continuously supplied to the *in vitro* testing, inducing the nucleation of small HAp particles on the surfaces of the previously formed particles rather than the radial growth of large HAp grains during prolonged soaking. The SEM micrograph of the 28-days soaked sample also revealed the crack formed on the new HAp layer. It was because the SBF induced HAp layer was porous structure, therefore, the shrinkage of this layer would occur when the soaked sample was taken out from the SBF solution and dried at room temperature. This drying shrinkage induced the crack formation in the HAp layer rather than the peeling off from composite surface, implying the strong adhesion between the SBF induced HAp layer and the composite surface.

3.5 *Compressive strength of HAp/PEA-co-PET composites*

Figure 7 shows load-deformation curves of HAp templates and HAp/PEA-*co*-PET composites. The HAp/PEA-*co*-PET composites show higher load-bearing and more plastic deformation than the HAp templates. Compressive strength and compressive modulus of the HAp/PEA-*co*-PET composites were 29 ± 2 MPa and 246 ± 5 MPa, respectively which distinctly increased from those of the porous HAp templates, i.e. 10 ± 1 MPa and 97 ± 4 MPa, respectively. The improvement of mechanical properties was ascribed to the presence of ROP-PEA-*co*-PET copolyester in the porous structure. This soft aliphatic part present in this copolyester could act as the load absorber, while the hard aromatic part could increase strength and stiffness of the HAp/PEA-*co*-PET composites.

The compressive strengths of the HAp/PEA-*co*-PET composites are higher than the compressive strength of cancellous bone, i.e. 2–13 MPa (Shors and Holmes 1993). This result suggested the possibility of usage of these composites as an implant material.

4. Conclusions

Cyclic oligo(ethylene adipate)-*co*-oligo(ethylene terephthalate) (C-OEA-*co*-C-OET) was successfully ring-opening polymerized in the porous of HAp templates at a temperature of 250 °C for 24 h under vacuum, resulting in the HAp/PEA-*co*-PET hybrid composite. The ROP-PEA-*co*-PET in the composites was characterized to be random copolyester. The increment of the compressive strength and compressive modulus presence of the HAp/PEA-*co*-PET composite was attributed to the presence of ROP-PEA-*co*-PET copolyester in the porous HAp template. The HAp/PEA-*co*-PET composite could induce the formation of hydroxyapatite nanocrystals after soaking in SBF solution, indicating the *in vitro* bioactivity of this composite.

Acknowledgement

The authors are thankful to the Thailand Research Fund (TRF) and the Commission on Higher Education (CHE), Ministry of Education, for financial support.

References

Antikainen T, Ruuskanen M, Taurio R, Kallioinen M, Serlo W, Törmälä P and Waris T 1992 *Acta Neurochir.* **117** 59

Chen Y, Mak A F T and Wang M 2007 *Key Eng. Mater.* **334–335** 1213

Chung H J, Kim H K, Yoon J J and Park T G 2006 *Pharm. Res.* **23** 1835

Ezhova Zh A, Koval E M, Zakharov N A and Kalinnikov V T 2011 *Russ. J. Inorg. Chem.* **56** 841

Ge H, Zhao B, Lai Y, Hu X, Zhang D and Hu K 2010 *J. Mater. Sci. Mater. Med.* **21** 1781

Hayakawa T, Mochizuki C, Hara H, Fukushima T, Yang F, Shen H, Wang S and Sato M 2009 *J. Hard Tiss. Biol.* **18** 7

Joe C R and Kim B H 1990 *J. Mater. Sci.* **25** 1991

Kim S S, Park M S, Gwak S J, Choi C Y and Kim B S 2006 *Tissue Eng.* **12** 2997

Kitajima A, Tsukamoto M and Akedo J 2010 *J. Ceram. Soc. Jpn* **118** 417

Kokubo T and Takadama H 2006 *Biomaterials* **27** 2907

Monvisade P, Siriphannon P, Jermsungnern R and Rattanabodee S 2007 *J. Mater. Sci. Mater. Med.* **18** 1955

Park J B 1979 *Biomaterials: An introduction* (New York: Plenum Press) pp 104–112

Risbud M, Saheb D N, Jog J and Bhonde R 2001 *Biomaterials* **22** 1591

Shors C E and Holmes E R 1993 *An introduction to bioceramic* (eds) L L Hench and J Wilson (Singapore: World Scientific Publishing Co.) pp 181–198

Siriphannon P, Kameshima Y, Yasumori A, Okada K and Hayashi S 2002 *J. Biomed. Mater. Res.* **60** 175

Song J H, Kim H E and Kim H W 2008 *J. Mater. Sci. Mater. Med.* **19** 2925

Tham W L, Chow W S and Mohd Ishak Z A 2010 *J. Reinf. Plast. Compos.* **29** 2065

Touny H A, Bhaduri S and Brown W P 2010 *J. Mater. Sci. Mater. Med.* **21** 2533

Vainionpää S 1985 *Arch. Orthop. Traum. Su.* **104** 333

Wahl D A, Sachlos E, Liu C and Czernuszka T J 2007 *J. Mater. Sci. Mater. Med.* **18** 201